IEEE Access
Multidisciplinary ⋮ Rapid Review ⋮ Open Access Journal

Received October 13, 2020, accepted October 27, 2020, date of publication October 30, 2020, date of current version November 12, 2020.

Digital Object Identifier 10.1109/ACCESS.2020.3034984

A Deep Learning Approach for Multi-Depth Soil Water Content Prediction in Summer Maize Growth Period

JINGXIN YU[1,2], SONG TANG[3], LILI ZHANGZHONG[2], WENGANG ZHENG[2], LONG WANG[4], (Member, IEEE), ALEXANDER WONG[5], (Senior Member, IEEE), AND LINLIN XU[1,5], (Member, IEEE)

[1]School of Land Science and Technology, China University of Geosciences, Beijing 100083, China
[2]National Engineering Research Center for Information Technology in Agriculture, Beijing 100097, China
[3]National Agricultural Technology Extension and Service Center, Beijing 100125, China
[4]School of Computer and Communication Engineering, University of Science and Technology Beijing, Beijing 100083, China
[5]Department of Systems Design Engineering, University of Waterloo, Waterloo, ON N2L 3G1, Canada

Corresponding authors: Linlin Xu (linlinxu618@gmail.com) and Wengang Zheng (zhengwg59@163.com)

This work was supported in part by the National Key Research and Development Program of China under Grant 2016YFD0300201-3, in part by the Modern Agro-Industry Technology Research System of Maize under Grant CARS-02-87, and in part by the Innovation Ability Construction Project of Beijing Academy of Agriculture and Forestry Sciences under Grant KJCX20180703.

ABSTRACT Advance knowledge of soil water content (SWC) in the soil wetting layer of crop irrigation can help develop more reasonable irrigation plans and improve the efficiency of agricultural irrigation water use. To improve the accuracy of predicting SWC at multiple depths, the ResBiLSTM model was proposed, in which continuous meteorological and SWC data were gridded and transformed as model inputs, and then high-dimensional spatial and time series features were extracted by ResNet and BiLSTM, respectively, and integrated by a meta-learner. Meteorological, SWC and growth stage records data from seven typical maize monitoring stations in Hebei Province, China, during the 2016-2018 summer maize planting process were utilized for the training, evaluation and testing of the ResBiLSTM model, with model prediction targets set at 20cm, 30cm, 40cm and 50cm depths. Experimental results showed that: 1) ResBiLSTM model could achieve better model fit and prediction of meteorological and SWC data at all growth stages, with R^2 within [0.818, 0.991], average MAE within [0.79%, 2.00%], and the overall prediction accuracy ranked as follows: anthesis maturity stage > seedling stage > tassel stage; 2) The average MSE of the ResBiLSTM model for the prediction of SWC in the next 1-6 days was within [3.91%, 15.82%], and the prediction accuracy decreased with the extension of the prediction time; 3) Compared with the classical machine learning model and related deep learning models, the ResBiLSTM model was able to obtain better prediction accuracy performance.

INDEX TERMS ResNet, BiLSTM, soil water content, growth stage, summer maize.

I. INTRODUCTION

Agricultural water consumption accounts for about 60% of economic and social water consumption in China, and the demand for efficient use of water resources in agriculture is becoming more and more urgent [1]. Maize is a major grain crop in China, with China National Bureau of Statistics announcing total maize production of 260.77 million tons in 2019, and Hebei Province is one of the major maize producing areas. Moisture in the soil is the main source of water uptake by crop roots, so knowing the trends of soil water content (SWC) at different depths of the corn irrigation wet layer in advance can help farms make a reasonable irrigation plan to improve water use efficiency [2]. However, due to changes in field meteorology, soil composition and crop growth at different growth stages, the SWC fluctuations show a complex non-linear relationship. In addition, modelling of data during the growth period of a crop can lead to more targeted models and better prediction accuracy [3]. The water consumption characteristics of crops also differ significantly

The associate editor coordinating the review of this manuscript and approving it for publication was Massimo Cafaro.

at different growth stages [4]. Therefore, it is important to construct a more accurate model for predicting SWC in the soil wetting layer for the maize growth stages.

Changes of SWC are mainly influenced by environmental factors such as evapotranspiration, groundwater, runoff, rainfall and other environmental factors on farmland, so in the early days it was often based on water balance or soil water dynamics to simulate soil water transfer for prediction [5]. For example, the FAO-developed crop-water productivity model AquaCrop, which simulated time-series changes in soil moisture by combining crop water consumption characteristics, irrigation regimes, and environmental evapotranspiration [6]. The Hydrus model, developed by the Saline Soil Laboratory, simulated changes in SWC by calculating moisture and solute transport patterns in the air pocket [7]. However, the mechanism models need to fully consider the water transport mechanism, soil characteristics, meteorological conditions and crop characteristics and other factors, the parameter rate setting process is complex and the rate setting model is only applicable to a single area and crop, limiting the promotion and application of the method in actual production [8].

With advances in sensor measurement technology, researchers can obtain extensive, continuous and reliable data on at in-situ monitoring sites [8]. The increase in data volume and quality allows machine learning algorithms to take advantage of the ability to fit complex non-linear relationships to build data-driven models [9]. Hong *et al.* [10] combined support vector machine (SVM) and relevance vector machine (RVM) to construct a predictive model for SWC over the next few days. Prasad *et al.* [11] used an extreme learning machine (ELM) model for predicting the average monthly SWC. However, traditional machine learning models are usually more restrictive in terms of sample quality and quantity, require more effort in data pre-processing and feature extraction, and have insufficient model generalization capability.

Artificial intelligence models based on artificial neural networks (ANN) can better mine the hidden features of big data and are an important direction of machine learning [12]. Chen *et al*. [13] combined principal component analysis (PCA) and radial basis function (RBF) neural networks to construct a SWC prediction model for tobacco fields. Yang *et al.* [14] proposed a hybrid algorithm combining discrete wavelet decomposition, BP neural network and particle swarm to construct a time series prediction model for SWC. Saha *et al.* [15] and Chatterjee *et al.* [16] used the Levenberg-Marquard back propagation method and flower pollination algorithm (MFPA) as training algorithms to train ANN to predict SWC, respectively. Increased neural network depth can improve model expression and optimization rate [17]. Cai *et al.* [18] constructed a model for predicting SWC for the next day using a deep neural network regression algorithm (DNNR) based on meteorological and 0-20 cm depth SWC data from three stations in Beijing, China. However, current ANN models for SWC prediction are usually single data feature extraction, without considering the spatial and temporal characteristics of the data, so it is difficult to achieve better prediction results. In addition, existing SWC prediction models usually only predict the surface layer (0-20 cm) or a single depth, which is hard to satisfy the actual agricultural irrigation decisions.

Convolutional neural network (CNN) was first proposed by LeCun [19]. The features of local area awareness, temporal domain up-sampling and weight sharing make CNN widely used in the field of image and video data classification. However, an increase in the number of layers of CNN leads to gradient disappearance while a decrease in the number of layers results in poor feature extraction [20]. To address the above problems, He *et al.* [21] proposed the residual network (ResNet), which introduced the residual block to build deep networks. On the other hand, the recurrent neural network (RNN) is better at modeling time series data and performs well in natural language processing [22]. To overcome the problem of gradient disappearance or gradient explosion that may occur with the long-range memory of the original RNN, Hochreiter and Schmidhuber [23] proposed the LSTM network based on the RNN by introducing a gate mechanism to update the information. However, LSTM can only learn forward features but ignores the learning of backward features, and the Bi-directional LSTM (BiLSTM) network built by combining forward and backward LSTMs can make better use of contextual semantic features [24]. The findings of [25], [26] for arrhythmia classification showed that ResNet and BiLSTM models were able to obtain better predictions compared to the independent CNN and LSTM models.

The spatio-temporal feature extraction advantage of integrating CNN and LSTM to construct a high-precision prediction model is a research hotspot [27]. For field environmental data, the combination of SWC and meteorological data over multiple consecutive days can be viewed as a two-dimensional, single-channel grayscale image, so the fusion model can use both CNN to extract high-dimensional features from the image [28] and LSTM to extract time-series features [29]. In other areas of research targeting regression prediction problems, Qin *et al.* [30] and Li *et al.* [31] constructed prediction models for PM2.5 by integrating CNN and LSTM structures, respectively, and obtained better performance compared to traditional machine learning models and independent CNN and LSTM models. Choi *et al.* [32] and Guo and Chen [33] constructed a short-term load forecasting model and a facial expression recognition model based on ResNet and LSTM, respectively. Zhou *et al.* [34] and Chen [35] applied the integrated model of ResNet and BiLSTM to heartbeat classification and network intrusion detection, respectively. However, few studies have constructed SWC prediction models by integrating the structures of ResNet and BiLSTM.

To overcome the drawbacks of existing methods, we propose a novel approach. Our motivation was to construct a novel SWC prediction model ResBiLSTM by combining the advantages of ResNet and BiLSTM for high-dimensional residual feature and time-series bidirectional

feature extraction, based on the ideas of integrated learning and previous research results. The meteorological, SWC and growth records data at seven sites in Hebei Province, China, were used to construct a multi-depth SWC prediction model for the soil wetting layer during the summer maize growth period. Hence, the main contributions of this work are listed next:

(1) Developed a prediction model ResBiLSTM for soil moisture content at different depths in agricultural fields by integrating the temporal and spatial feature extraction advantages of ResNet and BiLSTM models.

(2) Combined data from different growth stages of summer maize to reveal the differences in the fit ability and prediction accuracy of the ResBiLSTM model for different growth stage data.

(3) Analyzed the autocorrelation characteristics of soil water content at different depths in the field and compared the ability of the ResBiLSTM model to predict different days in the future.

(4) Compared and analyzed the predictive accuracy advantages of the ResBiLSTM integrated model over traditional machine learning and related deep learning models.

The remaining sections of this paper are organized as follows. Section II introduces the methods and materials, the methods part contains the construction principles of ResNet, BiLSTM, and ResBiLSTM models as well as the model evaluation methods and model training parameters, and the materials part contains the study area, data acquisition, data processing, and data analysis. Section III presents and discusses the predictive accuracy results of the ResBiLSTM model for different growth stages, different day delays, and different model comparisons, respectively, as well as the further study. Finally, conclusions are given in Section IV.

II. METHODS AND MATERIALS

The ResBiLSTM SWC prediction model was based on the idea of integrated learning by integrating the ResNet-based and BiLSTM-based models, and achieved the prediction capability of multi-depth SWC changes by integrating the high-dimensional residual features and bidirectional time series features of the matrix composed of SWC and meteorological data. Therefore, in this section, the principles of ResNet and BiLSTM, the ResBiLSTM model integration strategy, the model training evaluation strategy, and the model validation data were introduced, respectively.

A. ResNet

ResNet is built on a foundation of convolutional arithmetic, which extracts informative features by fusing spatial and channel-wise information within local receptive fields [21]. The core module of ResNet is the residual block, the structure of which is shown in Figure 1a, where x is the input, H(x) is the output, F(x) is the residual mapping function, weight layer is the convolution layer, BN represents the batch normalization layer, and ReLU represents the activation layer. The model is difficult to fit the actual mapping H(x) directly, so ResNet converts the problem to fitting the residual mapping F(x) by introducing ''skip connection'', so that the actual mapping H(x) can be expressed as $H(x) = F(x) + x$, which enables the model to approach the actual mapping by minimizing the residual function $F(x) = H(x) - x$ to solve the performance degradation problem of network stacking. Assuming that there are L layers of residual block connections, the output of the l-th residual block can be represented as

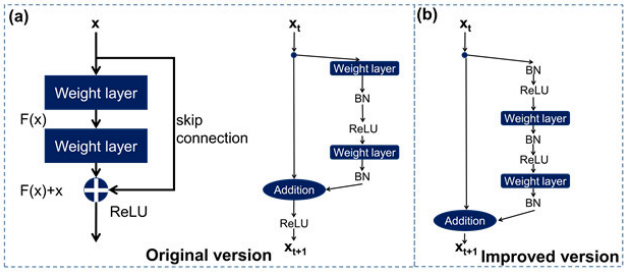

FIGURE 1. Structural diagram of the original and improved ResNet residue blocks.

$$x^{(l+1)} = x^{(l)} + \sum_{i=1}^{L-1} F\left(x^{(i)} + W^{(i)}\right) \quad (1)$$

where $x^{(l)}$ denotes the input of the l-th residual block, $x^{(l+1)}$ denotes that the output of this residual block is also the input of the $l+1$ th residual block, and $W^{(i)}$ is the convolution operation.

From (1), each layer of the residual network is accumulating the residual features of the upper layer, ensuring that layer $l+1$ always has more information about the features than layer l. In the process of back propagation, the error loss term is calculated for the gradient of the l-th residual block of the network according to the chain derivation rule as

$$\begin{aligned}\frac{\partial loss}{\partial x^{(l)}} &= \frac{\partial loss}{\partial x^{(L)}}\frac{\partial x^{(L)}}{\partial x^{(l)}} \\ &= \frac{\partial loss}{\partial x^{(L)}}\left(1 + \frac{\partial}{\partial x^{(l)}}\sum_{i=1}^{L-1} F\left(x^{(i)} + W^{(i)}\right)\right) \quad (2)\end{aligned}$$

An improved residual block structure was used in this study (Figure 1b), which differed from the original version in that gradients in the modified residual block could be directly connected to any earlier layer via shortcuts, thus solving the problem of gradients disappearing or exploding when training deeper networks [20].

During model training, internal covariate shift is caused by changes in the data distribution of internal nodes. The Batch Normalization (BN) layer is used to solve the problem of uneven and inconsistent data distribution in deep neural networks. The BN layer can speed up the training of deep neural networks. It normalizes the data after the activation function performs a non-linear transformation on the input data of the previous layer, so that the neural network maintains the consistency of the input data distribution, ensures the trainability of the network, reduces the large changes in the internal distribution of the network, speeds up the convergence

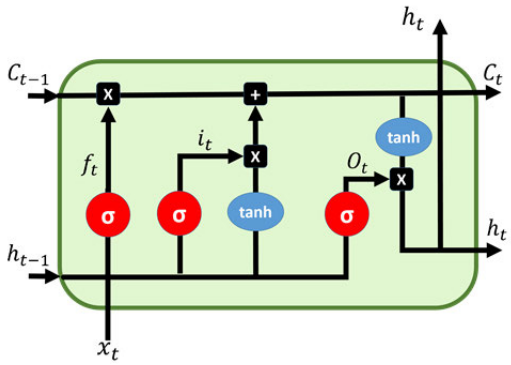

FIGURE 2. Schematic diagram of the memory unit structure of the LSTM network.

rate of the network and maintains the characterization ability of the neural network. As an activation function, Rectified Linear Unit (ReLU) had the sparse activation characteristic to avoiding the occurrence of overfitting. The mathematical expression is as

$$f(x) = \max(0, x) \tag{3}$$

B. BI-DIRECTIONAL LSTM

The LSTM structure is a variant of RNN structure, and its basic constituent unit is the Memory Unit (Figure 2), which can realize the functions of forgetting, remembering and outputting through the gate structure. By using the previous hidden state h_{t-1} and the current input x_t, it is possible to calculate the forgetting gate f_t, memory gate i_t and output gate o_t and then control the information state. By retaining important information and forgetting unimportant information, the Memory Unit eliminates the gradient explosion or gradient disappearance problem that exists with RNN.

The variables are calculated as (4)-(9).

Calculate the oblivion gate f_t from h_{t-1} and x_t by

$$f_t = \sigma(W_f x_t + U_f h_{t-1} + b_f) \tag{4}$$

Calculate memory gate i_t from h_{t-1} and x_t by

$$i_t = \sigma(W_i x_t + U_i h_{t-1} + b_i) \tag{5}$$

Calculate memory state $\tilde{C}_t$ from h_{t-1} and x_t by

$$\tilde{C}_t = \tanh(W_c x_t + U_c h_{t-1} + b_c) \tag{6}$$

Calculate the current memory state C_t from f_t, i_t, C_t and the previous moment memory C_{t-1} by

$$C_t = f_t * C_{t-1} + i_t * \tilde{C}_t \tag{7}$$

Calculate the output gate O_t from h_{t-1} and x_t by

$$O_t = \sigma(W_o x_t + U_o h_{t-1} + b_o) \tag{8}$$

Calculate the hidden state h_t at the current moment from o_t and C_t by

$$h_t = o_t * \tanh(C_t) \tag{9}$$

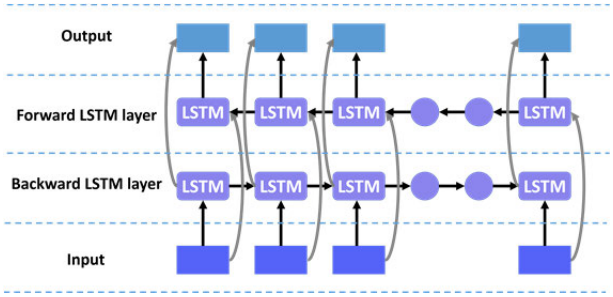

FIGURE 3. BiLSTM network structure diagram.

where, $W_f, U_f, W_i, U_i, W_c, U_c, W_o, U_o$ are weight matrices; b_f, b_i, b_c, b_o are bias vectors; tanh is hyperbolic tangent activation functions; σ is sigmoid activation functions.

BiLSTM is a combination of forward LSTM and backward LSTM and its structure is shown in Figure 3. Assuming that the hidden state of the output of the forward LSTM at time t is $\vec{h}_t$ and the hidden state of the output of the backward LSTM is $\overleftarrow{h}_t$, the hidden state h_{tb} of the output of the BiLSTM can be represented as

$$h_{tb} = \vec{h}_t \oplus \overleftarrow{h}_t \tag{10}$$

C. RESBILSTM

The ResBiLSTM model integrates two branches to extract spatio-temporal features of the data. The extracted spatio-temporal features are further learned by the meta-learner to achieve better data fitting capabilities.

Figure 4 shows the network structure of the ResBiLSTM model. The gridded SWC and meteorological time series data are input to the ResNet branch and BiLSTM branch, respectively, which are then integrated and learned through a meta-learner, with Adam used as the iterative optimization algorithm for model training and MSE used as the loss function.

By combining continuous multi-depth SWC and meteorological data, several successive time series data can be transformed into a two-dimensional matrix. The gridded data matrix with the multi-depth SWC and meteorological variables from left to right, and the time series from far to near from top to bottom. The gridded time series data can be represented as

$$X_{s,t} = \begin{Bmatrix} x_{1,t-n} & x_{2,t-n} & x_{3,t-n} & \cdots & x_{s,t-n} \\ x_{1,t-n+1} & x_{2,t-n+1} & x_{3,t-n+1} & \cdots & x_{s,t-n+1} \\ x_{1,t-n+2} & x_{2,t-n+2} & x_{3,t-n+2} & \cdots & x_{s,t-n+2} \\ \vdots & \vdots & \vdots & \ddots & \vdots \\ x_{1,t} & x_{2,t} & x_{3,t} & \cdots & x_{s,t} \end{Bmatrix} \tag{11}$$

where $X_{s,t}$ is the matrix of input items, s is the number of input variables, and t is the historical time step.

In the ResNet branch, the gridded data is first input to the 2D convolution layer, then connected to 2 consecutive residual blocks, and the output is flattened and connected to

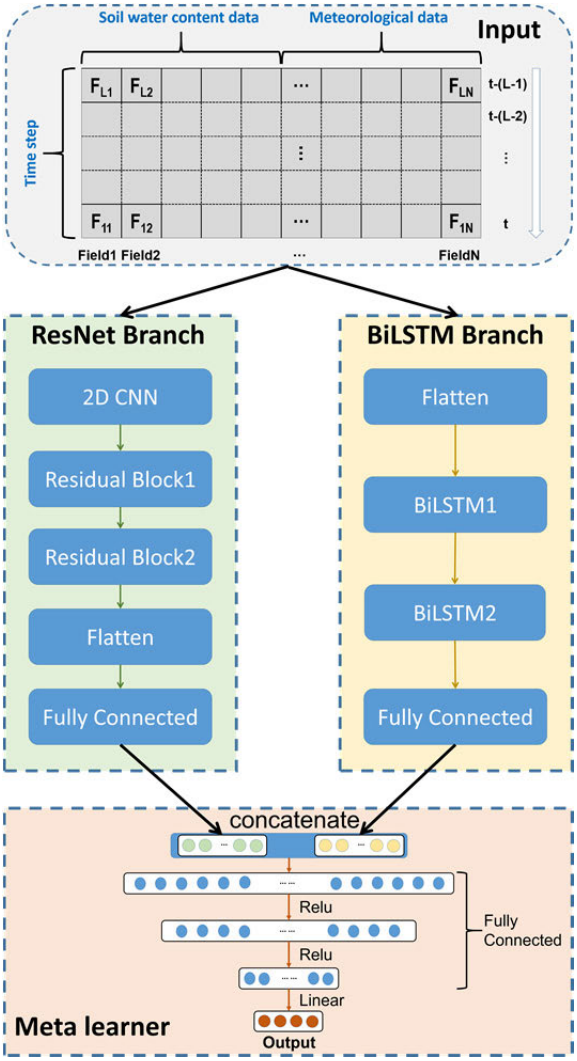

FIGURE 4. ResBiLSTM model network structure.

the full connection layer of 64 filters. Considering the small size of the input items compared to the photos, the model is stacked with 2 layers of residual blocks to ensure sufficient information is extracted and to make the model lightweight. 2D CNN layer has 64 feature maps and 3 × 3 convolution kernel size. 2D CNN layer has the same configuration with 64 filters and 3 × 3 convolution kernel size for both residual blocks.

In the BiLSTM branch, the input items are first flattened and then fed into two successive BiLSTM layers and finally output to a fully connected layer of 64 filters. The stacking of the two BiLSTM layers corresponds to a trend prediction on top of the prediction at each time step, thus allowing for a better representation of the time domain features.

Fully connected layers are adopted to construct a meta-learner for further learning of the feature parameters extracted from the ResNet branch and BiLSTM branch. 128 neurons from the two branches are first spliced to form a dense layer of 256 neurons, then three dense layers are connected, each with 128, 64 and 32 neurons, respectively.

The activation functions of all feature layers in the ResNet branch and BiLSTM branch use the ReLU function to mitigate overfitting. The output layer in the meta-learner uses the linear activation function.

D. LOSS FUNCTION AND MODEL TRAINING

Five evaluation measures were selected to indicate the performance of the different models.

Mean Squared Error (MSE) is

$$\mathrm{MSE} = \frac{1}{m}\sum_{i=1}^{m}\left(y_i - \hat{y}_i\right)^2 \tag{12}$$

Mean Absolute Error (MAE) is

$$\mathrm{MAE} = \frac{1}{m}\sum_{i=1}^{m}\left|\left(y_i - \hat{y}_i\right)\right| \tag{13}$$

Root Mean Squared Error (RMSE) is

$$\mathrm{RMSE} = \sqrt{\frac{1}{m}\sum_{i=1}^{m}\left(y_i - \hat{y}_i\right)^2} \tag{14}$$

Mean Absolute Percentage Error (MAPE) is

$$\mathrm{MAPE} = \frac{100}{n}\sum_{i=1}^{n}\left|\frac{\hat{y}_i - y_i}{y_i}\right| \tag{15}$$

Coefficient of determination (R^2) is

$$R^2 = 1 - \frac{\sum_i \left(\hat{y}_i - y_i\right)^2}{\sum_i \left(\overline{y_i} - y^i\right)^2} \tag{16}$$

In the above formula, is the predicted value, $\hat{y}_i$ is the true value, and $\overline{y_i}$ is the average value. MAE can reflect the actual situation of the predicted value error. MSE is the expected value of the square of the difference between the estimated and the observed value, it can evaluate the degree of the data change, and the smaller value of the MSE, the better accuracy of the prediction model. RMSE is the arithmetic square root of MSE. MAPE is equivalent to normalizing the error at each point, reducing the impact of the absolute error from individual outliers. R^2 can eliminate the influence of dimension on the evaluation measure.

The abstract process of training for models is shown as Figure 5. In addition, the specific training steps in this paper can be summarized as follows:

(1) The whole growth data are divided into separate data sets according to growth stage.

(2) The data are processed, including removal of outliers (such as null values, values beyond common sense, etc.), data normalization, and model input item construction.

(3) The processed data is randomly divided into training, validation, and test sets for model training, parameter tuning, and model testing, respectively.

(4) The Early Stopping method determines the timing of the model's termination of training based on the validation set results.

(5) The model after training uses the test set data to evaluate the model performance.

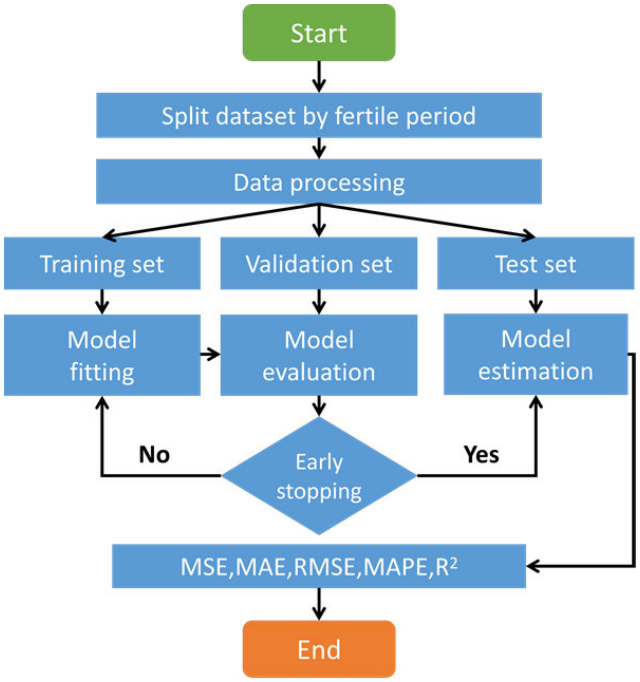

FIGURE 5. ResBiLSTM model training process.

The training environment for the research experiments was CPU: Intel(R) Xeon(R) CPU E5-1620 v4 @ 3.50GHz, GPU: NVIDIA Quadro K2200 and RAM: 32GB. The model training adopted Anaconda platform as the deep learning training base platform, Keras as the deep learning model building framework, and TensorFlow-gpu 1.13 was used at the back end to achieve parallel computing through CUDA technology to make full use of GPU resources to speed up training. Adam as an optimizer. To prevent the overfitting problem caused by too many model training sessions, this study adopted the early stopping method to determine the termination point of model training, and terminates the model training when the validation set error was not further reduced for 50 consecutive sessions, adopted the best performing model weights in the training process and saved the trained model as .h5 format.

E. STUDY AREA AND DATA ACQUISITION

The study area is Hebei Province, China (36°05′ −42°40′ N, 113°27′ −119°50′ E), which has a temperate continental monsoon climate with 2303.1 annual sunshine hours, 81-204 frost-free days, 484.5 mm of average annual precipitation, the distribution of precipitation is more southeast than northwest.

The data source was the China Meteorological Data Network (http://data.cma.cn). Considering the maize cultivation, soil, and meteorological factors, after communicating with the local agricultural authorities, a total of 2144 data from 7 maize-growing agro-meteorological monitoring stations in Hebei Province (Gaoyi Station, Feixiang Station, Dingzhou Station, Bazhou Station, Luoxian Station, and Huanghua Station) from 2016 to 2018 was selected as experimental data. Figure 6 shows the distribution of the stations.

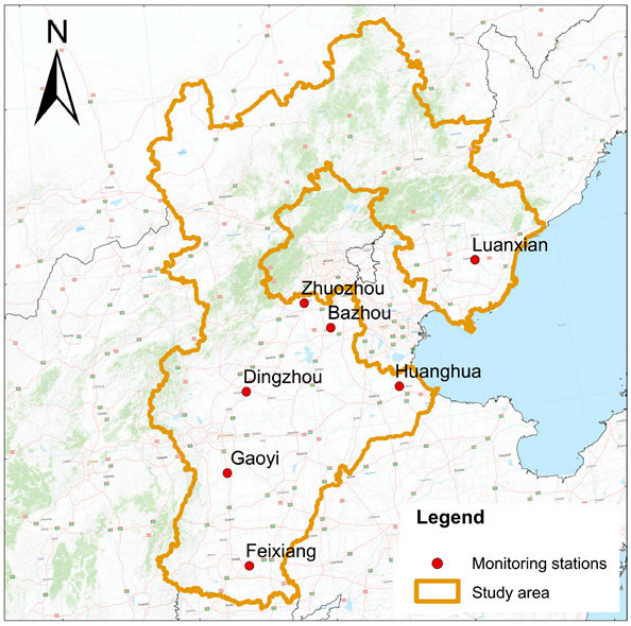

FIGURE 6. Research area and distribution of meteorological and soil moisture monitoring stations.

The selected sites had similar soil, climate and growth conditions. Meteorological and SWC data were determined by automatic meteorological moisture monitoring stations placed in maize fields with a frequency of 1 h, while crop growth data were determined and recorded by agricultural professionals based on crop phenotypic characteristics. The type of SWC used is the volumetric SWC (%). Daily averages of SWC at 10, 20, 30, 40 and 50 cm soil depths (SWC10, SWC20, SWC30, SWC40 and SWC50) were obtained. The meteorological data include daily average air temperature (Tmean, °C), daily minimum air temperature (Tmin, °C), daily maximum air temperature (Tmax, °C), daily average ground surface temperature (GTmean, °C), daily minimum ground surface temperature (GTmin, °C), daily maximum ground surface temperature (GTmax, °C), daily hours of sunshine (SSH, h), daily cumulative rainfall (pr, mm), daily average wind speed at 2m (U2, $m \cdot s^{-1}$) and daily average air humidity (RH, %). Crop growth data recorded the beginning and end of the ten growth stages of summer maize planted at each site.

F. DATA PROCESSING

Ten growth stages of summer maize in the raw data were divided into three growth stages. The seedling stage is a stage of nutritional growth that mainly focuses on root growth and leaf differentiation, including the sowing, seedling emergence, trifoliate and tiller stages, which generally lasts about 30 days. The tassel stage is the stage of nutritional growth and fertile growth in parallel, including pulling, gestation and tasseling stages, which generally lasts about 25-28 days. At the anthesis maturity stage, maize enters reproductive growth, including flowering, milk ripening and maturity stages, which usually lasts about 45-55 days. Table 1 shows

TABLE 1. Time periods for each growth stage of summer maize in 2016, 2017 and 2018.

Station	Year	Seedling stage	Tassel stage	Anthesis maturity stage	Station	Year	Seedling stage	Tassel stage	Anthesis maturity stage
Gaoyi	2018	06.13-07.02	07.03-08.04	08.05-09.20	Zhuozhou	2018	06.20-07.10	07.11-08.07	08.08-09.27
	2017	06.11-07.04	07.05-08.06	08.07-09.24		2017	06.17-07.06	07.07-08.09	08.10-09.29
	2016	06.13-07.04	07.05-08.04	08.05-09.22		2016	06.19-07.07	07.08-08.08	08.09-09.22
Feixiang	2018	06.02-06.30	07.01-08.03	08.04-09.12	Dingzhou	2018	06.07-07.02	07.03-08.06	08.07-09.18
	2017	06.03-07.02	07.03-08.03	08.04-09.20		2017	06.06-07.04	07.05-08.06	08.07-09.19
	2016	06.10-07.06	07.07-07.30	07.31-09.16		2016	06.10-07.02	07.03-08.06	08.07-09.18
Luanxian	2018	06.20-07.08	07.09-08.10	08.11-09.24	Bazhou	2018	06.11-07.04	07.05-08.05	08.06-09.22
	2017	06.17-07.08	07.09-08.08	08.09-09.17		2017	06.10-06.30	07.01-08.01	08.02-09.24
	2016	06.19-07.10	07.11-08.12	08.13-09.28		2016	06.12-07.02	07.03-08.03	08.04-09.26
Huanghua	2018	06.11-06.27	06.28-08.04	08.05-09.27					
	2017	06.25-07.12	07.13-08.16	08.17-10.06					
	2016	06.19-07.12	07.13-08.12	08.13-10.04					

the start and end times of each growth stage for the seven sites in 2016, 2017, and 2018, with relatively consistent planting periods for successive years of maize at the same site, and gradual delays in planting and harvesting of maize from south to north by climate, with a maximum difference of 23 days.

To make the best use of deep learning algorithms and fully exploit the value of the data, all meteorological and SWC variables were used for model construction to obtain the best prediction results. A study by Zhou *et al.* [36] on the optimal root zone soil moisture vertical regulation scheme had indicated that the maximum depth of the planned irrigated wet layer for maize planting was 50 cm. Considering the root growth of maize at different growth stages, the SWC at 20, 30, 40 and 50 cm depths was used as the prediction target. In addition, considering the convenience of model parameter design and practical application, the SWC and meteorological variables of the last three consecutive days were used to form the input matrix. Therefore, the input shape of the ResBiLSTM model is 15×3 and the output shape is 4×1.

For the data set division, the data of five sites were utilized for the model training, evaluation, and testing, 80% of modeling data was utilized for model training, 20% for model testing. In the data used for model training, 20% of it was randomly selected as validation data set to judge the model fitting. In addition, data normalization can improve the prediction accuracy and the fitting speed of model. Accordingly, the Min-Max normalization method was utilized to process each feature variable, and the data normalization formula is

$$x_{norm} = \frac{x_0 - x_{min}}{x_{max} - x_{min}} \tag{17}$$

where x_{norm}, x_0, x_{min}, and x_{max} are the normalized, real, minimum, and maximum values, respectively.

G. DATA ANALYSIS

Table 2 shows the mean, standard deviation (SD), maximum (Max), minimum (Min), and median values of SWC during different growth periods. Overall, the mean values of SWC are 19.06%, 25.44% and 25.24% at the seedling, tassel and anthesis maturity stages, respectively, and the minimum values of SWC for the entire growth period occurred at the seedling stage, while the maximum values occurred at the tassel stage. The standard deviations of SWC in each layer are within [7.6%, 9.1%], [8.25%, 10.2%] and [7.3%, 9.4%] at different growth stages, respectively, and SWC data are more discrete at the tassel stage than at the seedling and anthesis maturity stages, which make it more difficult to fit the tassel stage data effectively.

Table 3 presents the results of the statistical analysis of 10 meteorological variables. The time selected is the summer maize growth period, which is in summer, with long sunshine hours and relatively high air temperature and ground surface temperature. Seasonal factors also make the effect of crop transpiration and soil water evaporation obvious, which accelerate the process of SWC dissipation and bring uncertainty to the model prediction.

Table 4 shows the results of Pearson correlation analysis among the variables. The correlation coefficients between SWC at different depths are all above 0.5, showing a strong positive correlation. The correlations between the meteorological variables and SWC are different, with Tmean, Tmin, RH, pr, and GTmin showing positive correlations for SWC at different depths, and Tmax, GTmean, and GTmax showing negative correlations for SWC at different depths.

Figure 7 presents the results of the autocorrelation analysis of the prediction targets at different days delay. The autocorrelation coefficients for SWC at depths of 20, 30, 40, and 50 cm were within [0.962, 0.772], [0.968, 0.810], [0.977, 0.859], [0.984, 0.902], respectively, for a delay of 1-6 days, while the average of the autocorrelation coefficients for each layer was 0.973, 0.941, 0.912, 0.886, 0.861 and 0.836, respectively. The autocorrelation coefficient decreases with increasing number of delay days and increases with increasing soil depth within the same number of delay days.

TABLE 2. Statistical analysis results of soil water content at different soil depths.

Growth stage	Samples	Indicator	Mean	SD	Min	Max	Median
Seedling stage	472	SWC10 (%)	15.9	8.7	2.1	40.5	15.4
		SWC20 (%)	17.8	8.3	0.8	38	15.9
		SWC30 (%)	22.2	7.6	9.8	38.4	20.8
		SWC40 (%)	22.9	8.4	11.2	41.4	21.2
		SWC50 (%)	16.5	9.1	4.1	41.4	15.1
Tassel stage	676	SWC10 (%)	21.6	9.4	1.1	46.5	22.3
		SWC20 (%)	23.4	8.8	2.0	41.8	26.4
		SWC30 (%)	29.1	8.2	6.3	53.7	29.1
		SWC40 (%)	30.2	9.0	6.2	56.1	30.8
		SWC50 (%)	22.9	10.2	6.0	47.3	20.3
Anthesis maturity stage	996	SWC10 (%)	19.8	8.4	3.0	45	19.4
		SWC20 (%)	22.4	8.0	2.6	39.9	24.2
		SWC30 (%)	28.9	7.3	12.1	53	29.6
		SWC40 (%)	30.9	7.6	15.3	55.6	31.1
		SWC50 (%)	24.2	9.4	8.1	47.2	23.2
Entire growth period	2144	SWC10 (%)	19.1	9.1	2.1	46.5	19.2
		SWC20 (%)	21.2	8.6	0.8	41.8	23.1
		SWC30 (%)	26.7	8.1	9.8	53.7	28.0
		SWC40 (%)	28.1	8.8	11.2	56.1	29.2
		SWC50 (%)	21.2	9.6	4.1	47.3	20.1

TABLE 3. Results of statistical analysis of meteorological data throughout the entire growth period.

Variables	Mean	SD	Min	Max	Median
Tmean (℃)	25.9	3.2	14.9	33.7	26.3
Tmax (℃)	31.2	3.6	19.0	40.8	31.5
Tmin (℃)	21.4	3.6	7.5	29.1	22.0
RH (%)	72.8	14	24	100	76
pr (mm)	3.3	12.3	0	181.4	0
U2 ($m \cdot s^{-1}$)	1.7	0.9	0.2	6.7	1.5
SSH (h)	6.7	4.5	0	14.3	8.0
GTmean (℃)	29.7	4.3	18.3	42.4	29.6
GTmax (℃)	46.0	9.1	19.8	71.6	46.0
GTmin (℃)	20.7	3.9	4.0	28.3	21.3

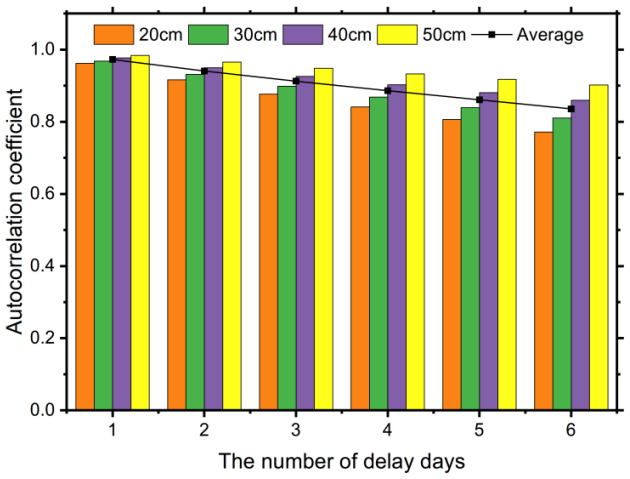

FIGURE 7. Autocorrelation analysis of soil water content at different days delay.

III. RESULTS AND DISSCUSSION

A. COMPARISON OF ResBiLSTM MODEL PREDICTION ACCURACY AT DIFFERENT GROWTH STAGES

ResBiLSTM model was used to train and validate the model on the data of the three growth stages separately. Figure 8 shows the results of the correlation between the predicted and true values of the test set at different depths for the three growth stages. The coefficients of determination R^2 were within [0.881, 0.987], [0.818, 0.926], and [0.944, 0.991] for the seedling, tassel, and anthesis maturity stages, respectively. The best fit of the model to the data at the anthesis maturity stage was obtained at 50 cm depth, with an R^2 of 0.991. The fit of the model at both the seedling and anthesis maturity stages increased with increasing soil depth. The degree of fit at different depths at the tassel stage was low and unstable, with the lowest degree of fit at 20 cm depth, with an R^2 of 0.818.

Table 5 presents the prediction accuracy of the ResBiLSTM model for different growth stages. The prediction accuracy of the model was ranked as: anthesis maturity stage > seedling stage > tassel stage. The average MSE, MAE, RMSE and MAPE of different depths at seedling stage and anthesis maturity stage were within [1.36%, 8.33%] and [0.68%, 3.98%], and the prediction accuracy tended to increase gradually with the increase of soil depth. The MSE at tassel stage was within [8.52%, 12.09%] and the average

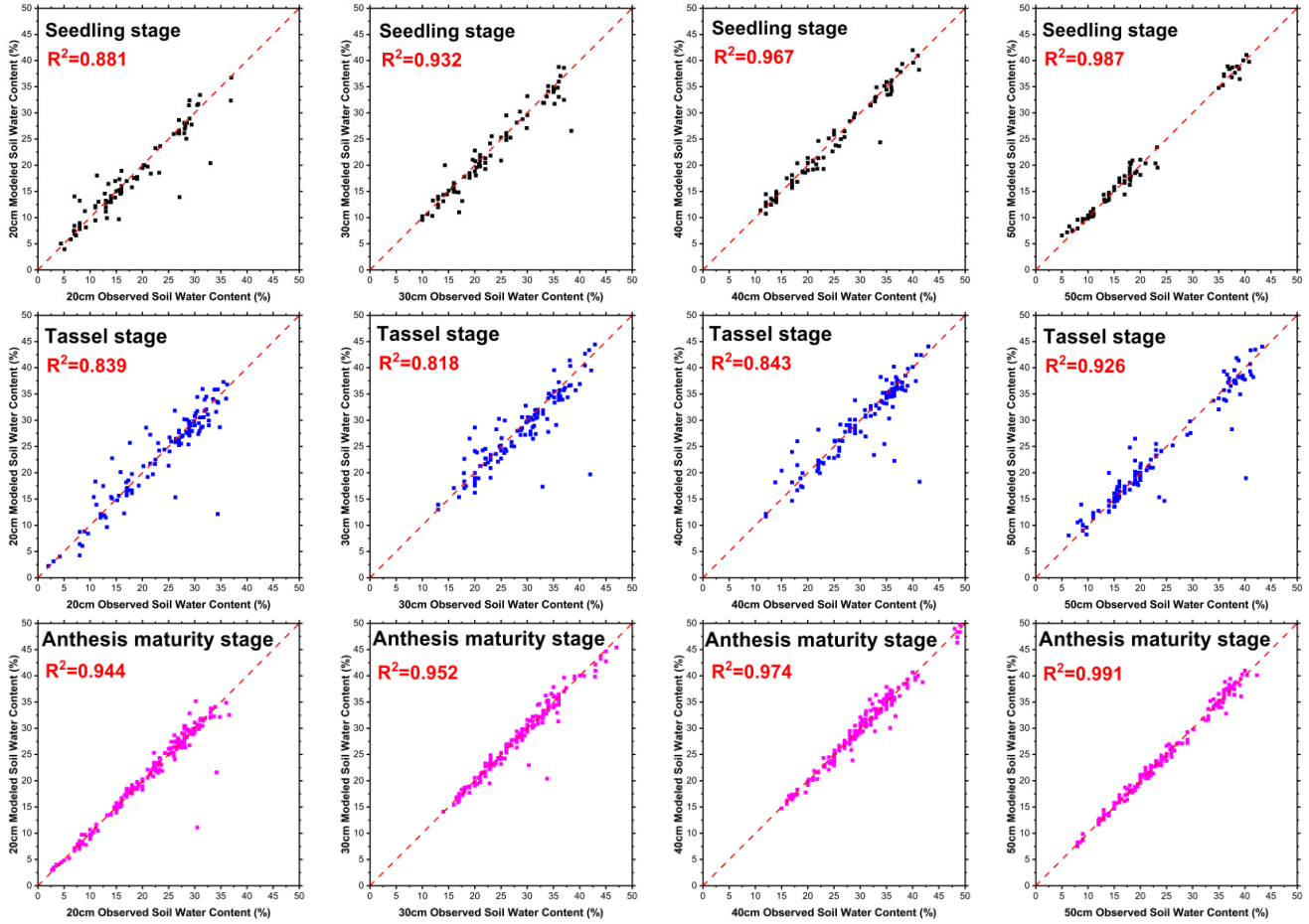

FIGURE 8. Comparison of model predicted and real values of soil water content at four soil depths for different growth stages.

TABLE 4. Results of Pearson correlation analysis of soil water content at different depths with other variables.

	SWC10	SWC20	SWC30	SWC40	SWC50	Tmean	Tmax	Tmin	RH	pr	U2	SSH	GTmean	GTmax	GTmin
SWC10	1	0.673	0.840	0.732	0.652	0.001	-0.127	0.141	0.346	0.267	0.099	-0.164	-0.139	-0.281	0.160
SWC20	0.673	1	0.701	0.510	0.623	0.085	-0.056	0.209	0.231	0.201	0.006	-0.115	-0.059	-0.200	0.197
SWC30	0.840	0.701	1	0.898	0.726	0.038	-0.079	0.152	0.269	0.181	0.013	-0.065	-0.071	-0.179	0.148
SWC40	0.732	0.510	0.898	1	0.587	0.010	-0.057	0.084	0.280	0.128	-0.005	-0.084	-0.059	-0.140	0.107
SWC50	0.652	0.623	0.726	0.587	1	0.004	-0.107	0.109	0.121	0.098	0.049	0.002	-0.114	-0.181	0.071

MSE at tassel stage was 7.29% and 9.48% higher than that at seedling stage and anthesis maturity stage, respectively. In addition, the MSE at 20, 30, and 40 cm depth at the tassel stage were close and exceeded 11%.

From Figure 8, the R^2 of all results was greater than 0.8, indicating that the model could fit the SWC data at multiple depths in different growth stages well. However, the R^2 was significantly lower at the tassel stage than at the seedling and anthesis maturity stage, and this trend was also evident in the MSE, MAE, RMSE, and MAPE in Table 5. This may be due to the fact that the standard deviations of different soil depths at the tassel stage ranged within [8.2%, 10.2%], whereas those at the seedling and anthesis maturity stages were within [7.6%, 9.1%] and [7.3%, 9.6%], respectively (Table 2), reflecting the fact that SWC data were more discrete among individuals at the tassel stage, making it more difficult to fit the model to the data. The study of Zhai *et al.* [4] showed that the increase in temperature at the tassel stage, plant nutritional growth was vigorous and water consumption intensity was maximum, where the water consumption modulus of maize ranged from 16.60%-35.26% and the water consumption intensity of maize ranged from 2.38-7.55 mm·d^{-1}. Study of maize irrigation regime also showed that the crop water requirement was highest at tassel stage and irrigation frequency was high [37]. The effect of crop water consumption and irrigation practices on SWC at

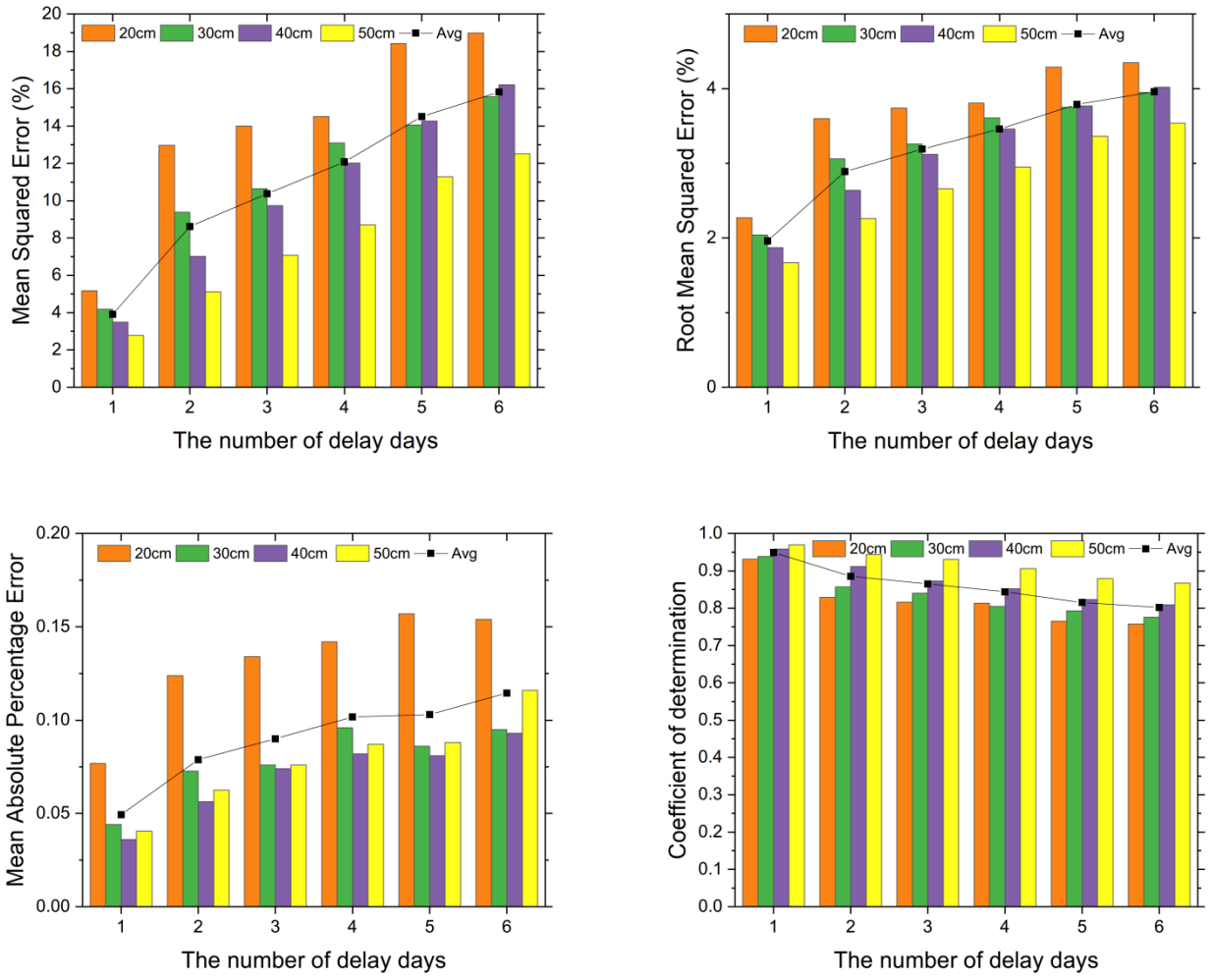

FIGURE 9. Comparison of the prediction accuracy of the ResBiLSTM model for soil water content at different soil depths for the next 1-6 days.

different depths made model predictions more difficult [38]. In addition, a study by Zhou *et al.* [36] showed that maize roots were mainly distributed at the depth of 0-40 cm, with shallow roots having a higher density and water uptake intensity than deeper roots, and differences in root uptake depth may also be responsible for the decrease in prediction accuracy with increasing depth.

B. COMPARISON OF PREDICTION ACCURACY WITH DIFFERENT DAYS DELAY

To compare the prediction accuracy for different days in the future, data from the entire growth period were used to train the model to predict SWC at different depths for the next 1-6 days, respectively. Figure 9 shows the error indicator values for the model's prediction of SWC at depths of 20, 30, 40, and 50 cm with 1-6 days delay. Soil depths ranged from shallow to deep with MSE within [5.17%, 18.98%], [4.19%, 15.57%], [3.49%, 16.21%], [2.78%, 12.52%] and RMSE within [2.27%, 4.35%], [2.04%, 3.95%], [1.87%, 4.02%], [1.67%, 3.54%]. MAPE were within [7.7%, 15.4%], [4.4%, 9.5%], [3.6%, 9.3%], [4.1%, 11.6%]. R^2 were within [0.757, 0.931], [0.776, 0.939], [0.809, 0.958], [0.867, 0.969]. The prediction accuracy of the model decreased with increasing prediction day delay and the model's prediction accuracy increased with increasing soil depth. Averaging the values of the error indicators at different depths, from shallow to deep MSE, RMSE, MAPE, and R^2 were within [3.91%, 15.82%], [1.96%, 3.54%], [4.9%, 11.5%], and [0.802, 0.949], respectively.

The model prediction accuracy evaluation indicators MSE, RMSE, MAPE, and R^2 showed a trend of decreasing prediction accuracy with increasing number of prediction days. This may be due to the fact that the correlation of SWC decreases over time, which is supported by the analysis of the autocorrelation coefficients of SWC at different depths for the next 1-6 days in Figure 7. The analysis of the autocorrelation of SWC from 1 to 16 days in the study of Cai *et al.* [18] was consistent

TABLE 5. The accuracy of the ResBiLSTM model for predicting soil water content at different growth stages and soil depths.

Growth stage	Depth (cm)	Test set MSE	MAE	RMSE	MAPE	Mean MSE	MAE	RMSE	MAPE
Seedling stage	20	8.33	1.70	2.89	11.2	4.27	1.26	2.07	7.0
	30	4.94	1.39	2.22	6.8				
	40	2.61	1.07	1.62	4.9				
	50	1.36	0.90	1.16	5.6				
Tassel stage	20	12.09	2.09	3.48	11.1	11.56	2.00	3.39	8.1
	30	12.23	2.16	3.49	8.1				
	40	11.56	1.91	3.40	7.1				
	50	8.52	1.63	2.92	8.0				
Anthesis maturity stage	20	3.98	0.91	1.99	5.3	2.08	0.79	1.44	3.2
	30	2.32	0.87	1.52	3.2				
	40	1.37	0.81	1.17	2.7				
	50	0.68	0.59	0.82	2.5				

with the findings of this study. In addition, Table 3 showed that the average daily rainfall during the growth period of summer maize was 3.3 mm, while the standard deviation and median rainfall were 12.3 mm and 0 mm, respectively. Since SWC is directly affected by irrigation and rainfall, the uncertainty of rainfall makes the probability of SWC being affected by rainfall increases with the number of days delay, which increases the difficulty of accurate prediction by the model.

From the perspective of different soil depths, the model's prediction accuracy for the 20 cm depth was much lower than for the 30 cm, 40 cm and 50 cm depths, which may be due to the fact that shallow soils were more affected. According to Table 4, the correlation coefficients of daily precipitation with SWC20 and SWC50 were 0.202 and 0.098, respectively, with the shallow layers being more affected. Furthermore, the maximum surface temperature was directly related to soil water evaporation [39]. The correlation coefficients of GST with SWC20 and SWC50 were −0.201 and −0.182, respectively, also proving that shallow layers are more susceptible to environmental factors. The study of temporal and spatial variability of soil by Alun *et al.* [40] also showed that the variability of SWC decreased with increasing soil depth, which is consistent with the findings of this study.

C. COMPARISON OF PREDICTIVE ACCURACY OF DIFFERENT MODELS

To demonstrate the advantages of the ResBiLSTM model in terms of SWC prediction accuracy, the performance of classical machine learning models in SWC prediction, such as Support Vector Regression (SVR) [41], Multi-Layer Perceptron (MLP) [42] and Random Forest (RF) [43] were compared. Also, the ResBiLSTM model was based on the integrated model of ResNet and BiLSTM, so two new models by removing the ResNet branch and the BiLSTM branch were constructed, respectively. In addition, the DNNR [18], CNN-LSTM1 [30], and CNN-LSTM2 [31] mentioned in the introductory section were selected as the deep learning models involved in the comparison. The same data set partitioning and model training strategy was used for all tested models.

Table 6 shows the prediction accuracy results of different models for the same data set. The MAPE of all the models involved were less than 10%, indicating that these models were able to make good predictions. The ResBiLSTM model had the best prediction accuracy with MSE, MAE, MAPE and RMSE of 3.90%, 1.02%, 4.5% and 1.94%, respectively. The proposed ResBiLSTM model has a significant prediction accuracy advantage over the traditional machine learning models (SVR, MLP and RF). The ResBiLSTM model reduced MSE by 23.1% and 16.8% compared to the independent ResNet and BiLSTM branches, respectively. Compared to the related deep learning models, the ResBiLSTM model presents better prediction accuracy with a 14.3% and 13.7% decrease in MSE compared to the CNN-LSTM1 and CNN-LSTM2 models, respectively.

TABLE 6. Prediction accuracy of soil water content by different models.

Model	Test set MSE	MAE	MAPE	RMSE
SVR	9.67	2.05	9.2	3.11
MLP	8.31	2.07	10.0	2.88
RF	7.76	1.71	8.7	2.78
DNNR	5.13	1.26	5.7	2.22
ResBiLSTM without ResNet	5.07	1.30	6.3	2.23
ResBiLSTM without BiLSTM	4.69	1.18	5.1	2.07
CNN-LSTM2	4.55	1.14	5.1	2.05
CNN-LSTM1	4.52	1.18	5.6	2.07
ResBiLSTM (proposed)	**3.90**	**1.02**	**4.5**	**1.94**

The prediction accuracy of deep learning models was better than those of classical machine learning models (SVR, MLP, and RF). The deep learning model's ability to mine potential features of the data is key to its ability to provide a better fit to complex nonlinear data. Cai *et al.* [18] compared the prediction accuracy of the DNNR model with some classical machine learning models, the results were consistent with this study. Meanwhile, the prediction accuracy of the spatiotemporally integrated models (ResBiLSTM, CNN-LSTM1 and CNN-LSTM2) is higher than that of the independent models (ResBiLSTM without ResNet and ResBiLSTM without BiLSTM), which indicates that by combining the spatially high dimensional features extracted by CNN and the time-series features extracted by LSTM, the models can obtain better feature extraction capability and thus better prediction accuracy compared to the individual models. Li *et al.* [31] and Qin *et al.* [30] investigated the construction of PM2.5 prediction models by integrating CNN and LSTM, and the results

showed that combining time-domain and spatial-domain features resulted in better prediction accuracy, which had the same conclusion as this study. In addition, the proposed ResBiLSTM model has the best prediction accuracy performance, which indicates that the addition of residual blocks and the application of bidirectional LSTM after the convolutional layer further enhances the model's spatio-temporal feature extraction ability and further utilizes the meta-learner to learn spatio-temporal features to obtain better prediction accuracy. The findings of He *et al.* [25] and Huang *et al.* [26] for arrhythmia classification showed that combining ResNet and BiLSTM could improve the predictive ability of the model, which was similar to the findings of this study. The above advantages make the ResBiLSTM model particularly suitable for predicting soil water content at multiple depths during the summer maize growth period.

D. LIMITATIONS AND FURTHER STUDY

The ResBiLSTM model combined with the advantages of spatial and time series feature extraction, and obtained a good prediction accuracy for SWC. However, the ResBiLSTM model has some shortcomings in that it does not take into account the weather forecast in the composition of the inputs, which makes the model inadequate in predicting the process of the increase in the moisture of the surface soil. In addition, there is a need to improve the balance of data sets across growth periods. The following studies will be conducted in the future: 1) to increase the number of stations and extend the time series range; 2) to extend the types of data input to the model, such as soil and vegetation conditions, human activity, weather forecast information; 3) to optimize the model structure and parameter settings to achieve more efficient model training and better generalized prediction capability.

IV. CONCLUSION

The ResBiLSTM model was proposed for the multi-depth SWC model prediction in maize soil wetting layer, which integrates ResNet and BiLSTM based on the existing research. The model took the gridded meteorological and SWC data as inputs and extracted the spatially high dimensional features and time series features of the data to achieve a better prediction. Meteorological and multi-depth SWC data of summer maize growth stages in 2016, 2017 and 2018 at seven stations in Hebei Province, China, were selected as model training data. The experimental results showed that the ResBiLSTM model could achieve a good fit and prediction effect for different growth stages, and the prediction accuracy for different growth stages was ranked as: anthesis maturity stage > seedling stage > tassel stage. The accuracy of the ResBiLSTM model in predicting the multi-depth SWC for 1-6 days delay decreased as the prediction time increased. The deep learning model had better prediction accuracy than the traditional machine learning models (SVR, MLP and RF), and the ResBiLSTM model had the best prediction performance among the deep models involved in the comparison (DNNR, ResBiLSTM without ResNet, ResBiLSTM without BiLSTM, CNN-LSTM1 and CNN-LSTM2). This study has implications for the researches on soil water content prediction model construction and deep learning spatiotemporal feature model design.

REFERENCES

[1] X. Cao, J. Ren, M. Wu, X. Guo, and W. Wang, "Assessing agricultural water use effect of China based on water footprint framework," *Trans. Chin. Soc. Agric. Eng.*, vol. 34, no. 5, pp. 1–8, 2018.
[2] O. Adeyemi, I. Grove, S. Peets, Y. Domun, and T. Norton, "Dynamic neural network modelling of soil moisture content for predictive irrigation scheduling," *Sensors*, vol. 18, no. 10, p. 3408, Oct. 2018, doi: 10.3390/s18103408.
[3] M. K. Saggi and S. Jain, "Application of fuzzy-genetic and regularization random forest (FG-RRF): Estimation of crop evapotranspiration (ET) for maize and wheat crops," *Agricult. Water Manage.*, vol. 229, Feb. 2020, Art. no. 105907, doi: 10.1016/j.agwat.2019.105907.
[4] C. Zhai, H. Zhou, and J. Zhao, "Experimental study on inter-annual water requirement and water consumption of drip irrigation maize in north of Xinjiang," *Sci. Agric. Sin.*, vol. 50, no. 14, pp. 2769–2780, 2017.
[5] G. Egea, A. Diaz-Espejo, and J. E. Fernández, "Soil moisture dynamics in a hedgerow olive orchard under well-watered and deficit irrigation regimes: Assessment, prediction and scenario analysis," *Agricult. Water Manage.*, vol. 164, pp. 197–211, Jan. 2016, doi: 10.1016/j.agwat.2015.10.034.
[6] P. Steduto, T. C. Hsiao, D. Raes, and E. Fereres, "AquaCrop—The FAO crop model to simulate yield response to water: I. concepts and underlying principles," *Agronomy J.*, vol. 101, no. 3, pp. 426–437, May 2009.
[7] D. E. Radcliffe and J. Simunek, *Soil Physics With HYDRUS: Modeling and Applications*. Boca Raton, FL, USA: CRC Press, 2018.
[8] W. Zheng, L. Zhangzhong, X. Zhang, C. Wang, S. Zhang, S. Sun, and H. Niu, "A review on the soil moisture prediction model and its application in the information system," in *Computer and Computing Technologies in Agriculture XI*. Cham, Switzerland: Springer, 2019, pp. 352–364, doi: 10.1007/978-3-030-06137-1_32.
[9] A. Dey, "Machine learning algorithms: A review," *Int. J. Comput. Sci. Inf. Technol.*, vol. 7, no. 3, pp. 1174–1179, 2016.
[10] Z. Hong, Z. Kalbarczyk, and R. K. Iyer, "A data-driven approach to soil moisture collection and prediction," in *Proc. IEEE Int. Conf. Smart Comput. (SMARTCOMP)*, May 2016, pp. 1–6.
[11] R. Prasad, R. C. Deo, Y. Li, and T. Maraseni, "Soil moisture forecasting by a hybrid machine learning technique: ELM integrated with ensemble empirical mode decomposition," *Geoderma*, vol. 330, pp. 136–161, Nov. 2018.
[12] K. Liakos, P. Busato, D. Moshou, S. Pearson, and D. Bochtis, "Machine learning in agriculture: A review," *Sensors*, vol. 18, no. 8, p. 2674, Aug. 2018.
[13] C. Chen, J. Tan, J. Yin, F. Zhang, and J. Yao, "Prediction model for soil moisture in tobacco fields based on PCA and RBF neural network," *Trans. Chin. Soc. Agric. Eng.*, vol. 26, no. 8, pp. 85–90, 2010.
[14] X. Yang, C. Zhang, Q. Cheng, H. Zhang, and W. Gong, "A hybrid model for soil moisture prediction by using artificial neural networks," *Rev. Fac. Ing. UCV*, vol. 32, no. 5, pp. 265–271, 2017.
[15] S. Saha, F. Gu, X. Luo, and R. L. Lytton, "Prediction of soil-water characteristic curve for unbound material using Fredlund–Xing equation-based ANN approach," *J. Mater. Civil Eng.*, vol. 30, no. 5, May 2018, Art. no. 06018002.
[16] S. Chatterjee, N. Dey, and S. Sen, "Soil moisture quantity prediction using optimized neural supported model for sustainable agricultural applications," *Sustain. Comput., Informat. Syst.*, Sep. 2018, Art. no. 100279. [Online]. Available: https://www.sciencedirect.com/science/article/abs/pii/S2210537918302464?via%3Dihub
[17] K. Kawaguchi, J. Huang, and L. P. Kaelbling, "Effect of depth and width on local minima in deep learning," *Neural Comput.*, vol. 31, no. 7, pp. 1462–1498, Jul. 2019.
[18] Y. Cai, W. Zheng, X. Zhang, L. Zhangzhong, and X. Xue, "Research on soil moisture prediction model based on deep learning," *PLoS ONE*, vol. 14, no. 4, Apr. 2019, Art. no. e0214508, doi: 10.1371/journal.pone.0214508.
[19] Y. LeCun, "Generalization and network design strategies," *Connectionism Perspective*, vol. 19, pp. 143–155, Jun. 1989.
[20] K. He, X. Zhang, S. Ren, and J. Sun, "Identity mappings in deep residual networks," in *Proc. Eur. Conf. Comput. Vis.*, 2016, pp. 630–645.

[21] K. He, X. Zhang, S. Ren, and J. Sun, "Deep residual learning for image recognition," in *Proc. IEEE Conf. Comput. Vis. Pattern Recognit. (CVPR)*, Jun. 2016, pp. 770–778.
[22] J. T. Connor, R. D. Martin, and L. E. Atlas, "Recurrent neural networks and robust time series prediction," *IEEE Trans. Neural Netw.*, vol. 5, no. 2, pp. 240–254, Mar. 1994.
[23] S. Hochreiter and J. Schmidhuber, "Long short-term memory," *Neural Comput.*, vol. 9, no. 8, pp. 1735–1780, 1997.
[24] J. Zhou, Y. Lu, H.-N. Dai, H. Wang, and H. Xiao, "Sentiment analysis of Chinese microblog based on stacked bidirectional LSTM," *IEEE Access*, vol. 7, pp. 38856–38866, 2019.
[25] R. He, Y. Liu, K. Wang, N. Zhao, Y. Yuan, Q. Li, and H. Zhang, "Automatic cardiac arrhythmia classification using combination of deep residual network and bidirectional LSTM," *IEEE Access*, vol. 7, pp. 102119–102135, 2019.
[26] C. Huang, R. Zhao, W. Chen, and H. Li, "Arrhythmia classification with attention-based res-BiLSTM-net," in *Machine Learning and Medical Engineering for Cardiovascular Health and Intravascular Imaging and Computer Assisted Stenting*. Cham, Switzerland: Springer, 2019, pp. 3–10.
[27] T.-Y. Kim and S.-B. Cho, "Predicting residential energy consumption using CNN-LSTM neural networks," *Energy*, vol. 182, pp. 72–81, Sep. 2019.
[28] C. Huang, J. Zhang, L. Cao, L. Wang, X. Luo, J.-H. Wang, and A. Bensoussan, "Robust forecasting of river-flow based on convolutional neural network," *IEEE Trans. Sustain. Comput.*, early access, Mar. 30, 2020, doi: 10.1109/TSUSC.2020.2983097.
[29] J. Zhang, F. Chen, Z. Cui, Y. Guo, and Y. Zhu, "Deep learning architecture for short-term passenger flow forecasting in urban rail transit," *IEEE Trans. Intell. Transport. Syst.*, early access, Jul. 8, 2020, doi: 10.1109/TITS.2020.3000761.
[30] D. Qin, J. Yu, G. Zou, R. Yong, Q. Zhao, and B. Zhang, "A novel combined prediction scheme based on CNN and LSTM for urban PM2.5 concentration," *IEEE Access*, vol. 7, pp. 20050–20059, 2019, doi: 10.1109/ACCESS.2019.2897028.
[31] T. Li, M. Hua, and X. Wu, "A hybrid CNN-LSTM model for forecasting particulate matter (PM2.5)," *IEEE Access*, vol. 8, pp. 26933–26940, 2020, doi: 10.1109/ACCESS.2020.2971348.
[32] H. Choi, S. Ryu, and H. Kim, "Short-term load forecasting based on ResNet and LSTM," in *Proc. IEEE Int. Conf. Commun., Control, Comput. Technol. Smart Grids (SmartGridComm)*, Oct. 2018, pp. 1–6, doi: 10.1109/SmartGridComm.2018.8587554.
[33] H. Guo and J. Chen, "Dynamic facial expression recognition based on ResNet and LSTM," *IOP Conf. Series: Mater. Sci. Eng.*, vol. 790, Apr. 2020, Art. no. 012145, doi: 10.1088/1757-899X/790/1/012145.
[34] Y. Zhou, H. Zhang, Y. Li, and G. Ning, "ECG heartbeat classification based on ResNet and bi-LSTM," *IOP Conf., Earth Environ. Sci.*, vol. 428, Jan. 2020, Art. no. 012014, doi: 10.1088/1755-1315/428/1/012014.
[35] C. C. Hongsong, "Study on construction of IOT network intrusion detection classification model and optimization based on combination of ResNet and bidirectional LSTM network," *J. Hunan Univ. Nat. Sci.*, vol. 47, no. 8, pp. 1–8, 2020.
[36] S. Zhou, X. Hu, W. Wang, and Y. Zhang, "Water-saving and stable yield effects of regulation on soil wetted depth in different growth stage of spring maize," *Trans. Chin. Soc. Agric. Eng.*, vol. 32, no. 21, pp. 125–132, 2016.
[37] J. Guo, G. Yin, J. Gu, and Z. Liu, "Determination of irrigation scheduling of spring maize in different hydrological years in Fuxin, Liaoning Province based on CROPWAT model," *Chin. J. Ecol.*, vol. 35, no. 12, pp. 3428–3434, 2016.
[38] W.-Q. Yu, Y.-J. Wang, H.-B. Hu, Y.-Q. Wang, H.-L. Zhang, B. Wang, and Y. Liu, "Regulations and patterns of soil moisture dynamics and their controlling factors in hilly regions of lower reaches of yangtze river basin, China," *J. Central South Univ.*, vol. 22, no. 12, pp. 4764–4777, Dec. 2015.
[39] B. Ait Hssaine, O. Merlin, J. Ezzahar, S. Er-raki, S. Khabba, and A. Chehbouni, "Assessing soil moisture constraint on soil evaporation and plant transpiration fractioning," in *Proc. EGU Gen. Assem. Conf. Abstr.*, 2020, p. 8751.
[40] L. Alun, Y. Weizhong, and L. Juan, "Spatial analysis methods and application of regional soil moisture," *Chin. Agric. Sci. Bull.*, vol. 2012, no. 21, p. 60, 2012.
[41] J. Fan, W. Yue, L. Wu, F. Zhang, H. Cai, X. Wang, X. Lu, and Y. Xiang, "Evaluation of SVM, ELM and four tree-based ensemble models for predicting daily reference evapotranspiration using limited meteorological data in different climates of China," *Agricult. Forest Meteorol.*, vol. 263, pp. 225–241, Dec. 2018.
[42] X. Fan, L. Wang, and S. Li, "Predicting chaotic coal prices using a multi-layer perceptron network model," *Resour. Policy*, vol. 50, pp. 86–92, Dec. 2016.
[43] A. Liaw and M. Wiener, "Classification and regression by randomforest," *R News*, vol. 2, no. 3, pp. 18–22, 2002.

JINGXIN YU received the master's degree in cartography and geographic information systems from Beijing Forestry University in 2016. He is currently pursuing the Ph.D. degree with the School of Land Science and Technology, China University of Geosciences, Beijing, China. His research interest includes the development of soil moisture prediction models for the crops root zone incorporating multi-source data.

SONG TANG received the master's degree. He is currently a Senior Agronomist with the National Agricultural Technology Extension and Service Center, Beijing, China. His research interest includes soil water engineering domain.

LILI ZHANGZHONG received the Ph.D. degree in agricultural engineering from China Agricultural University in 2016. She is currently an Associate Researcher with the National Engineering Research Center for Information Technology in Agriculture, Beijing, China. Her research interest includes agricultural engineering domain.

WENGANG ZHENG received the Ph.D. degree in computational mechanics from the Dalian University of Technology, China, in 2002. He is currently a Professor with the National Engineering Research Center for Information Technology in Agriculture, Beijing, China. His research interest includes agricultural engineering domain.

LONG WANG (Member, IEEE) received the M.Sc. degree (Hons.) in computer science from University College London, London, U.K., in 2014, and the Ph.D. degree in systems engineering and engineering management from the City University of Hong Kong, Hong Kong, in 2017. He is currently an Associate Professor with the Department of Computer Science and Technology, University of Science and Technology Beijing, Beijing, China. His research interests include machine learning, computational intelligence, and computer vision and their industrial applications. He was a recipient of the Hong Kong Ph.D. Fellowship in 2014. He serves as an Associate Editor of IEEE Access and *Canadian Journal of Electrical and Computer Engineering*, as well as an Academic Editor of PLOS One. He is also a Lead Guest Editor of the Special Issue on Data Science of *Intelligent Automation and Soft Computing* and *Water*.

ALEXANDER WONG (Senior Member, IEEE) received the B.A.Sc. degree in computer engineering, the M.A.Sc. degree in electrical and computer engineering, and the Ph.D. degree in systems design engineering from the University of Waterloo, Waterloo, ON, Canada, in 2005, 2007, and 2010, respectively. He is currently the Canada Research Chair of Artificial Intelligence and Medical Imaging, the Co-Director of the Vision and Image Processing Research Group, an Associate Professor with the Department of Systems Design Engineering, University of Waterloo, and a member of the College of the Royal Society of Canada. He has authored over 450 refereed journal and conference papers and holds patents in various fields such as computational imaging, artificial intelligence, computer vision, graphics, image processing, and multimedia systems. His research interests include integrative biomedical imaging systems design, operational artificial intelligence, and scalable and explainable deep learning. He has received a number of awards, including two outstanding performance awards, the Distinguished Performance Award, the Engineering Research Excellence Award, the Sandford Fleming Teaching Excellence Award, the Early Researcher Award from the Ministry of Economic Development and Innovation, the Best Paper Awards by the Canadian Image Processing and Pattern Recognition Society in 2009 and 2014, the Distinguished Paper Award by the Society of Information Display in 2015, the Best Paper Award from the NIPS Workshop on Efficient Methods for Deep Neural Networks in 2016, the Best Paper Award from the NIPS Workshop on Transparent and Interpretable Machine Learning in 2017, the Best Paper Awards for the Conference on Computer Vision and Imaging Systems in 2015 and 2017, the AquaHacking Challenge First Prize in 2017, the Synaptive Best Medical Imaging Paper Award in 2016, two Magna Cum Laude Awards and one Cum Laude Award from the Annual Meeting of the Imaging Network of Ontario, the Best Student Paper from the Ottawa Hockey Analytics Conference in 2017, and the Alumni Gold Medal (based on document published in October 4, 2018).

LINLIN XU (Member, IEEE) received the B.Eng. and M.Sc. degrees in geomatics engineering from the China University of Geosciences, Beijing, China, in 2007 and 2010, respectively, and the Ph.D. degree in geography from the University of Waterloo, Waterloo, ON, Canada, in 2014. His current research interests include hyperspectral imaging, satellite remote sensing, machine learning, and artificial intelligence.